Refinement of the Nonplanar Aspects of the Subsonic Doublet-Lattice Lifting Surface Method

W. P. RODDEN,* J. P. GIESING,† AND T. P. KALMAN‡
Douglas Aircraft Company, McDonnell Douglas Corporation, Long Beach, Calif.

The initial formulation of the Doublet-Lattice Method has proven theoretically accurate for calculating the interference effects on arbitrary classes of oscillating nonplanar configurations with one known exception: nearly coplanar wing/horizontal-tail combinations. For this class of problems the integration of the kernel across the element loses accuracy. The reason for this loss of accuracy is explained, and a refined method for performing the required integration is presented. Numerical studies using wing-tail configurations are presented to illustrate how well the refined method works. Also a T-tail calculation is repeated to show that calculations using other configurations are unaffected by the refinement.

Nomenclature

A, B, C = coefficients in parabolic approximations to kernel numerators; subscripts 1 and 2 refer to planar and nonplanar parts of kernel, respectively
b_r = reference semichord
C_L = total lift coefficient
C_l = rolling moment coefficient; $C'_{l,\psi}$ is the rolling moment due to yaw of the horizontal stabilizer of Ref. 11 and Fig. 6
$\bar{c}$ = reference chord length
D_{rs} = normalwash factor; D_{0rs} is steady normalwash factor; D_{1rs} and D_{2rs} are incremental oscillatory, planar, and nonplanar normalwash factors, respectively; D_{Prs} is value of D_{1rs} for $\bar{z} = 0$
e = box semiwidth
F = integral in Eq (17); F_P is Mangler principal part for planar case
I_0 = integral defined in Eq. (8)
K = kernel function; K_1 and K_2 are factors in numerators of planar and nonplanar parts of kernel, respectively
$\mathfrak{K}_\nu(x)$ = modified Bessel function of argument x
k_r = reference reduced frequency, $k_r = \omega b_r/U$
M = Mach number
N = number of lifting surfaces
$P(\bar{\eta})$ = parabolic approximation to kernel numerator; P_1 and P_2 are approximations for planar and nonplanar numerators, respectively
r = cylindrical radius from sending doublet
S_n = area of nth lifting surface
$S.P.(\ )$ = denotes singular part of ( )
s = semispan
T = direction cosine function; T_1 and T_2 are functions for planar and nonplanar parts of kernel, respectively, and T_2* is modified value of T_2
U = freestream velocity
u_1 = parameter defined in Eq. (9)
$x_0, \bar{y}, \bar{z}$ = Cartesian coordinate system transformed to midpoint of sending line and aligned with plane of sending box; $\bar{z}$ is also vertical gap between near-coplanar parallel surfaces
ε = parameter defined in Eq. (31)
γ = dihedral angle; γ_r snd γ_s are dihedral angles of receiving and sending boxes, respectively, and $\bar{\gamma}_r = \gamma_r - \gamma_s$ is the relative dihedral angle between receiving and sending boxes
Δx_s = centerline chord of sending box
$\bar{\eta}$ = spanwise coordinate, in the plane of an element
ϕ = phase angle
λ_s = sweepback angle of sending box ¼-chord line
ψ = yaw angle
ω = circular frequency

Received March 8, 1971: revision received August 16, 1971. This paper was supported by the U. S. Air Force Flight Dynamics Laboratory under Contract F33615-70-C-1167 and by the Independent Research and Development (IRAD) Program of the McDonnell Douglas Corporation. Portions of this paper were included in a paper (Ref. 12) presented to the AGARD Symposium on Unsteady Aerodynamics for Aeroelastic Analyses of Interfering Surfaces, Tønsberg, Oslofjorden, Norway, November 3–4, 1970. The authors wish to acknowledge E. Albano of the Northrop Corporation, Aircraft Division, for his remarks on the behavior of the linear combination of the planar and nonplanar parts of the kernel.

Index categories: Nonsteady Aerodynamics; Subsonic and Transonic Flow; Aeroelasticity and Hydroelasticity.

* Consulting Engineer. Associate Fellow AIAA.

† Senior Group Engineer, Structural Mechanics Section. Associate Fellow AIAA.

‡ Engineer/Scientist, Structural Mechanics Section. Member AIAA.

Introduction

THE Doublet-Lattice Method (*DLM*)[1] is a finite-element method for the solution of the oscillatory subsonic pressure-normalwash integral equation for multiple interfering surfaces

$$w(x,s) = (1/8\pi) \sum_{n=1}^{N} \iint_{S_n} K(x,\xi;s,\sigma) p(\xi,\sigma) d\xi d\sigma \qquad (1)$$

where w is the complex amplitude of dimensionless normalwash, p is the complex amplitude of lifting pressure coefficient, (x,s) are orthogonal coordinates on the nth surface S_n such that the undisturbed stream is parallel to the x axis, and K is the complex acceleration potential kernel for oscillatory subsonic flow. The kernel has been given by Rodemich[2] and Landahl[3] in the form

$$K = \exp(-i\omega x_0/U)(K_1 T_1 + K_2 T_2)/r^2 \qquad (2)$$

where ω is the frequency, x_0 is the distance between the sending and receiving points parallel to the freestream, U is the velocity of the freestream

$$T_1 = \cos(\gamma_r - \gamma_s) \qquad (3)$$

$$T_2 = (1/r^2)(z_0 \cos\gamma_r - y_0 \sin\gamma_r)(z_0 \cos\gamma_s - y_0 \sin\gamma_s) \qquad (4)$$

$$r = (y_0^2 + z_0^2)^{1/2} \qquad (5)$$

y_0 and z_0 are the Cartesian distances between the sending and receiving points perpendicular to the freestream, and γ_r and γ_s are the dihedral angles at the receiving and sending points, respectively. The coordinate system is illustrated in Fig. 1. We find it convenient to refer to K_1 and K_2 as the planar and nonplanar parts of the kernel numerator, respectively, although both are obviously nonplanar in general. Then, the so-called planar and nonplanar parts are given by [2, 3]

$$K_1 = r(\partial I_0/\partial r) \qquad (6)$$

$$K_2 = r^3(\partial/\partial r)[(1/r)\partial I_0/\partial r] \qquad (7)$$

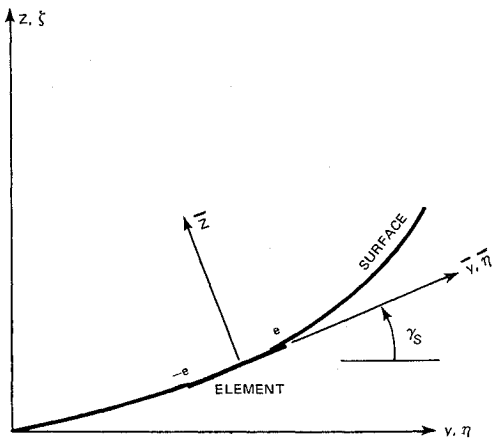

Fig. 1 Lifting surface coordinate system.

where the integral I_0 is

$$I_0 = \int_{u_1}^{\infty} \frac{\exp(-i\omega r u/U)}{(1+u^2)^{1/2}}\, du \tag{8}$$

in which

$$u_1 = \{M[x_0{}^2 + (1-M^2)r^2]^{1/2} - x_0\}/(1-M^2)r \tag{9}$$

and M is the Mach number. Expanded forms of K_1 and K_2 for computation are given by Landahl,[3] although their signs should be reversed.

The original method for determining the influence of an oscillating lifting surface element at a point was based on the assumption that the lifting pressure could be concentrated along a line. The line is located at the ¼-chord line of the element and the elements are formed by division of the surface(s) into small trapezoidal panels (boxes) arranged in strips parallel to the freestream and with surface edges, fold lines, and hinge lines located on box boundaries as in Fig. 2. The lifting load line is represented by a horseshoe vortex for its steady effects and a line of doublets for its incremental oscillatory effects. The surface boundary condition is a prescribed normalwash at the control point of each box which is located at the ¾-chord point along the centerline of each box. The numerical form of the integral equation, Eq. (1), in matrix notation becomes

$$\{w\} = [D]\{p\} \tag{10}$$

where the elements of the normalwash factor matrix $[D]$ are

$$D_{rs} = (\Delta x_s/8\pi) \int_{-e}^{e} K\, d\bar{\eta} \tag{11}$$

where Δx_s is the centerline chord of the sending box and e is its semi width, and the streamwise integration of the kernel has been performed by concentrating the lifting pressure at the ¼-chord load line. The spanwise integration was performed analytically by approximating the numerator of the kernel by a parabola

$$K \approx P(\bar{\eta})/r^2 \tag{12}$$

where $P(\bar{\eta})$ is the parabolic function of $\bar{\eta}$ determined by evaluating the numerator at the middle and both ends of the lifting line and fitting the second-degree curve through these points.

The initial formulation of the DLM has been found to be theoretically accurate for calculating interference effects on arbitrary nonplanar configurations[4] with one known exception: a near-coplanar wing/horizontal-tail combination. This configuration was tested for its flutter characteristics at the Cornell Aeronautical Lab. and analyzed by Balcerak,[5] Albano et al.,[6] and Giesing et al.[7] The configuration is shown in Fig. 3 along with results[8] from the original formulation of the *DLM* and the present refinement. The total lift coefficient (wing plus tail) is shown (based on total area of both surfaces) for plunging motion with a reduced frequency $k_r = \omega b_r/U = 0.6$ where $b_r = 0.41856s$ and at a Mach number $M = 0.7$. It is seen that the original algorithm starts to lose accuracy when the vertical gap-to-chord ratio is approximately 0.1, which is the width of the inboard eight strips. The reasons for the failure of the original *DLM* are discussed in the following sections.

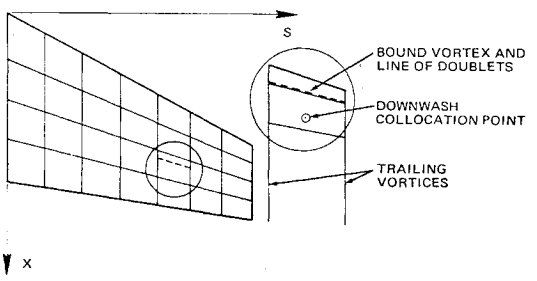

Fig. 2 Idealization of the lifting surface using trapezoidal boxes.

Refinement

The basic difficulty with the original approach, in the near-coplanar case, can be explained by considering the downstream character of the kernel for small r. When such a limit is taken, the numerator of the kernel approaches

$$P(\bar{\eta}) \to \{2\cos\bar{\gamma}_r - 4(\bar{z}/r)^2\cos\bar{\gamma}_r + 4[\bar{z}(\bar{y}-\bar{\eta})/r^2]\sin\bar{\gamma}_r\} \times \exp(-i\omega x_0/U) \tag{13}$$

where element coordinates (indicated by a bar over the quantities) are used having their origin located on the sending element and rotated into the plane of the element as shown in Fig. 1. The numerator is a well behaved function of $\bar{\eta}$ except when $\bar{z}$ approaches zero when $\bar{y} = 0$. Figure 4 presents plots of $\bar{z}^2/r^2$ and $\bar{z}\bar{\eta}/r^2$ vs $\bar{\eta}$ for various values of $\bar{z}$. It is seen that the variation of these functions with $\bar{\eta}$ becomes progressively larger as $\bar{z}$ approaches zero. For sufficiently small $\bar{z}$, a parabola cannot approximate accurately a linear combination of the two functions shown in Fig. 4 and the method fails. It should be noted, however, that the method is again valid for the planar case. It is therefore necessary to treat the planar and nonplanar parts of the kernel separately. We rewrite the expressions of Rodemich[2] and Landahl[3] for the kernel as

$$K = (K_1T_1/r^2 + K_2T_2{}^*/r^4)\exp(-i\omega x_0/U) \tag{14}$$

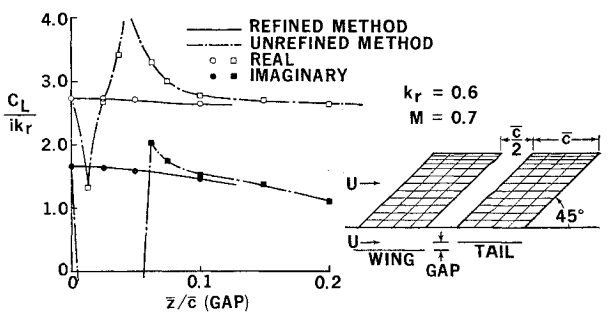

Fig. 3 Variation of total lift coefficient with vertical distance between wing and tail for plunging motion.

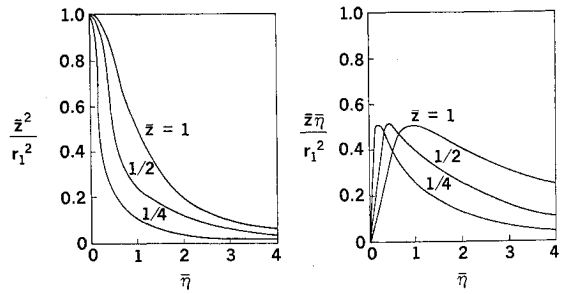

Fig. 4 Variation of the nonplanar part of the kernel across an element in the spanwise direction.

where

$$T_2^* = T_2 r^2 \tag{15a}$$

$$= \bar{z}^2 \cos\bar{\gamma}_r - \bar{z}\bar{y} \sin\bar{\gamma}_r \tag{15b}$$

The evaluation of the normalwash factor, Eq. (11) in element coordinates gives

$$D_{rs} = (\Delta x_s/8\pi) \int_{-e}^{e} (K_1 T_1/r^2 + K_2 T_2^*/r^4) \times \exp[-i\omega(x_0 - \bar{\eta}\tan\lambda_s)/U] d\bar{\eta} \tag{16}$$

where

$$r^2 = (\bar{y} - \bar{\eta})^2 + \bar{z}^2 \tag{17}$$

and λ_s is the sweep angle of the $\frac{1}{4}$-chord line of the sending box. The downwash factor is evaluated as before[1] by adding and subtracting the steady values of K_1 and K_2, denoted by K_{10} and K_{20}, respectively, to their oscillatory counterparts. Then, Eq. (16) becomes

$$D_{rs} = D_{0rs} + D_{1rs} + D_{2rs} \tag{18}$$

where

$$D_{0rs} = \frac{\Delta x_s}{8\pi} \int_{-e}^{e} \left\{ \frac{K_{10} T_1}{r^2} + \frac{K_{20} T_2^*}{r^4} \right\} d\bar{\eta} \tag{19}$$

$$D_{1rs} = \frac{\Delta x_s}{8\pi} \int_{-e}^{e} \frac{\{K_1 \exp[-i\omega(x_0 - \bar{\eta}\tan\lambda_s)/U] - K_{10}\} T_1}{r^2} d\bar{\eta} \tag{20}$$

$$D_{2rs} = \frac{\Delta x_s}{8\pi} \int_{-e}^{e} \frac{\{K_2 \exp[-i\omega(x_0 - \bar{\eta}\tan\lambda_s)/U] - K_{20}\} T_2^*}{r^4} d\bar{\eta} \tag{21}$$

Equation (19) is the steady downwash factor and is more conveniently derived from horseshoe vortex considerations than by evaluating the integral. The steady downwash factor has been given by Hedman.[9] We may evaluate the incremental oscillatory downwash factors [Eqs. (20) and (21)] in closed form by again approximating the numerators as parabolas. We rewrite Eq. (20) as

$$D_{1rs} = \frac{\Delta x_s}{8\pi} \int_{-e}^{e} \frac{P_1(\bar{\eta}) d\bar{\eta}}{(\bar{y} - \bar{\eta})^2 + \bar{z}^2} \tag{22}$$

where $P_1(\bar{\eta})$ is the parabolic approximation

$$P_1(\bar{\eta}) = A_1 \bar{\eta}^2 + B_1 \bar{\eta} + C_1 \tag{23a}$$

$$\approx \{K_1 \exp[-i\omega(\bar{x} - \bar{\eta}\tan\lambda_s)/U] - K_{10}\} T_1 \tag{23b}$$

If we denote the inboard, center, and outboard values of $P_1(\bar{\eta})$ by $P_1(-e)$, $P_1(0)$ and $P_1(e)$, respectively, the parabolic coefficients are

$$A_1 = [P_1(-e) - 2P_1(0) + P_1(e)]/2e^2 \tag{24}$$

$$B_1 = [P_1(e) - P_1(-e)]/2e \tag{25}$$

$$C_1 = P_1(0) \tag{26}$$

The planar downwash factor then becomes

$$D_{1rs} = (\Delta x_s/8\pi) \Big\{ [(\bar{y}^2 - \bar{z}^2) A_1 + \bar{y} B_1 + C_1] F + (\tfrac{1}{2} B_1 + \bar{y} A_1) \ln \left[\frac{(\bar{y} - e)^2 + \bar{z}^2}{(\bar{y} + e)^2 + \bar{z}^2} \right] + 2eA_1 \Big\} \tag{27}$$

where

$$F = \int_{-e}^{e} \frac{d\bar{\eta}}{(\bar{y} - \bar{\eta})^2 + \bar{z}^2} = \frac{1}{|\bar{z}|} \tan^{-1} \left(\frac{2e|\bar{z}|}{\bar{y}^2 + \bar{z}^2 - e^2} \right) \tag{28}$$

The term F may be rewritten as follows:

$$F = \delta_1 \frac{2e}{\bar{y}^2 + \bar{z}^2 - e^2} \left[1 - \varepsilon \left(\frac{\bar{z}^2}{e} \right) \right] + \delta_2 \frac{\pi}{|\bar{z}|} \tag{29}$$

where

$$\delta_1 = 1, \delta_2 = 0, \quad \text{for} \quad \bar{y}^2 + \bar{z}^2 - e^2 > 0 \tag{30a}$$

$$\delta_1 = 0, \delta_2 = \tfrac{1}{2}, \quad \text{for} \quad \bar{y}_2 + \bar{z}^2 - e^2 = 0 \tag{30b}$$

$$\delta_1 = 1, \delta_2 = 1, \quad \text{for} \quad \bar{y}^2 + \bar{z}^2 - e^2 < 0 \tag{30c}$$

in order to place the arctangent in the correct quadrant, and

$$\varepsilon = \frac{e^2}{|\bar{z}|^2} \left[1 - \frac{\bar{y}^2 + \bar{z}^2 - e^2}{2e|\bar{z}|} \tan^{-1} \left(\frac{2e|\bar{z}|}{\bar{y}^2 + \bar{z}^2 - e^2} \right) \right] \tag{31a}$$

and when $|2e\bar{z}/(\bar{y}^2 + \bar{z}^2 - e^2)| \leq 0.3$, the series expansion

$$\varepsilon = \frac{4e^4}{(\bar{y}^2 + \bar{z}^2 - e^2)^2} \sum_{n=2}^{7} \frac{(-1)^n}{2n-1} \left(\frac{2e\bar{z}}{\bar{y}^2 + \bar{z}^2 - e^2} \right)^{2n-4} \tag{31b}$$

has been used. It is seen immediately, for the cases $\bar{y}^2 + \bar{z}^2 e^2 \leq 0$, that F becomes singular like $\pi/|\bar{z}|$ and $\pi/2|\bar{z}|$, respectively. However, it will be shown that a similar contribution (of opposite sign) arises from the nonplanar part which exactly cancels this singular term. Thus, the usual practice for planar cases ($\bar{z} = 0$) is to evaluate the Mangler[10] principal part of F where these two singularities are cancelled analytically. The Mangler principal part is:

$$F_P = \int_{-e}^{e} \frac{d\bar{\eta}}{(\bar{y} - \bar{\eta})^2} = \left\{ \frac{1}{y - e} - \frac{1}{y + e} \right\} \tag{32}$$

The incremental nonplanar oscillatory downwash factor is evaluated by rewriting Eq. (21) as

$$D_{2rs} = \frac{\Delta x_s}{8\pi} \int_{-e}^{e} \frac{P_2(\bar{\eta}) d\bar{\eta}}{[(\bar{y} - \eta)^2 + \bar{z}^2]^2} \tag{33}$$

where $P_2(\eta)$ is another parabolic approximation

$$P_2(\bar{\eta}) = A_2 \bar{\eta}^2 + B_2 \bar{\eta} + C_2 \tag{34a}$$

$$\approx \{K_2 \exp[-i\omega(\bar{x} - \bar{\eta}\tan\lambda_s)/U] - K_{20}\} T_2^* \tag{34b}$$

Letting $P_2(-e)$, $P_2(0)$, and $P_2(e)$ denote the inboard, center, and outboard values of $P_2(\bar{\eta})$, respectively, we have

$$A_2 = [P_2(-e) - 2P_2(0) + P_2(e)]/2e^2 \tag{35}$$

$$B_2 = [P_2(e) - P_2(-e)]/2e \tag{36}$$

$$C_2 = P_2(0) \tag{37}$$

The nonplanar downwash factor is then evaluated to be

$$D_{2rs} = \frac{\Delta x_s}{16\pi\bar{z}^2} \Big\{ [(\bar{y}^2 + \bar{z}^2) A_2 + \bar{y} B_2 + C_2] F + \frac{1}{(\bar{y} + e)^2 + \bar{z}^2} \Big([(\bar{y}^2 + \bar{z}^2)\bar{y} + (\bar{y}^2 - \bar{z}^2)e] A_2 + (\bar{y}^2 + \bar{z}^2 + \bar{y}e) B_2 + (\bar{y} + e) C_2 \Big) - \frac{1}{(\bar{y} - e)^2 + \bar{z}^2} \Big([(\bar{y}^2 + \bar{z}^2)\bar{y} - (\bar{y}^2 - \bar{z}^2)e] A_2 + (\bar{y}^2 + \bar{z}^2 - \bar{y}e) B_2 + (\bar{y} - e) C_2 \Big) \Big\} \tag{38}$$

Equation (38) tends to lose significance for small values of $\bar{z}$. Introducing ε into Eq. (38) leads to

$$D_{2rs}=\frac{\Delta x_s e}{8\pi(\bar{y}^2+\bar{z}^2-e^2)}\left\{\frac{2(\bar{y}^2+\bar{z}^2+e^2)(e^2A_2+C_2)+4\bar{y}e^2B_2}{[(\bar{y}+e)^2+\bar{z}^2][(\bar{y}-e)^2+\bar{z}^2]}\right.$$
$$\left.-\frac{(\delta_1\varepsilon+\Delta)}{e^2}[(\bar{y}^2+\bar{z}^2)A_2+\bar{y}B_2+C_2]\right\} \quad (39)$$

where

$$\Delta=\left(\frac{e}{\bar{z}}\right)^2\left\{1-\delta_1-\delta_2\frac{\pi}{|\bar{z}|}\left(\frac{\bar{y}^2+\bar{z}^2-e^2}{2e}\right)\right\} \quad (40)$$

The simplification of Eq. (38) via Eq. (29) is somewhat tedious but results in the more accurate form in which ε is given by Eq. (31). Equations (39) and (40) are used in general except when $|\bar{y}^2+\bar{z}^2-e^2)/2e\bar{z}|<0.1$ in which case Eq. (38) is used.

When $\bar{y}^2+\bar{z}^2-e^2>0$, $\delta_1=1$ and $\delta_2=0$ and, therefore, $\Delta=0$. In this case no singularities arise in either D_{1rs} or D_{2rs} as $\bar{z}$ approaches zero. However, when the receiving point lies in the wake region of the sending element, (i.e., when $\bar{y}^2+\bar{z}^2-e^2<0$) then both D_{1rs} and D_{2rs} contain singularities. One of the basic requirements of the Doublet-Lattice Method is that streamwise strip edges must be aligned for all surfaces in the same or nearly the same plane. Thus, if a receiving point is in the wake of a sending element, it must be centered in that wake, and, therefore, $\bar{y}=0$. Under these circumstances, the limiting values of C_1 and C_2 are

$$C_1\to 2[\exp(-i\omega x_0/U)-1] \quad (41)$$

$$C_2\to -4\bar{z}^2[\exp(-i\omega x_0/U)-1] \quad (42)$$

from which

$$C_2\to -2C_1\bar{z}^2 \quad (43)$$

The singular parts of D_{1rs} and D_{2rs} are [referring to Eqs. (27) and (38)]

$$S.P.(D_{1rs})=(\Delta x_s/8\pi)(\pi/|\bar{z}|)C_1 \quad (44)$$

$$S.P.(D_{2rs})=(\Delta x_s/8\pi)(\pi/|\bar{z}|)(C_2/2\bar{z}^2) \quad (45)$$

When Eq. (43) is placed into Eq. (45) the singular parts of D_{1rs} and D_{2rs} cancel out. However, the cancellation of these singularities numerically will lead to difficulties for sufficiently small values of $\bar{z}$. The point at which inaccuracies occur depends on the number of significant figures carried in the computation. If eight significant figures are carried, then no difficulties have been observed down to $\bar{z}/e=0.001$. At this point, the problem may be assumed to be planar. Figure 5a shows that the nonplanar part proceeds smoothly to zero as

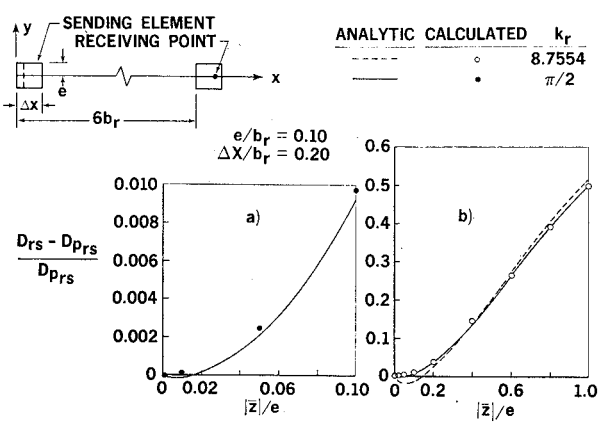

Fig. 5 Comparison of analytic and calculated results for the nonplanar part of the downwash factor.

$|\bar{z}|/e$ approaches zero. It is of interest to ascertain the accuracy of this approach to zero. Figures 5a and 5b present two example calculations for a receiving or collocation point lying in the wake of a sending element. The separation distance between the two is large enough to allow a simplified version of the kernel to be employed for the analytic calculation. Specifically

$$P_1(\bar{\eta})=2(\omega r/U)\Re_1(\omega r/U)\exp(-i\omega x_0/U)-2 \quad (46)$$

$$P_2(\bar{\eta})=-2(\omega r/U)^2\Re_2(\omega r/U)\exp(-i\omega x_0/U)+4 \quad (47)$$

where $\Re_1$ and $\Re_2$ are modified Bessel functions of first and second order. Evaluating A_1, C_1, A_2, and C_2 from Eqs. (24–26) and Eqs. (35–37) (note that $B_1=B_2=0$ since $\bar{y}=0$ and $\lambda_s=0$) while using the above simplified expressions for $P_1(\bar{\eta})$ and $P_2(\bar{\eta})$ gives the analytic and calculated nonplanar parts of the downwash factors normalized by the planar downwash factor. Figure 5b covers the range of $\bar{z}/e$ up to 1.0, while Fig. 5a presents the details of the curve ($k_r=\omega b_r/U=\pi/2$) near $\bar{z}/e$ of zero.

These curves illustrate several interesting points. First, note that the curves are relatively insensitive to the reduced frequency k_r. Expansion of the nonplanar part of the downwash factor shows that the dominant term is dependent on k_r only through the term $\exp(-ik_rx_0/b_r)$

$$D_{rs}-D_{Prs}=\frac{\Delta x_s}{8\pi}\frac{4(\bar{z}/e)^2}{1+(\bar{z}/e)^2}\exp(-ik_rx_0/b_r) \quad (48)$$

The term D_{Prs} is proportional to $\exp(-ik_rx_0/b_r)$ so $(D_{rs}-D_{Prs})/D_{Prs}$ has very little variation with k_r. The logarithmic terms inherent in the modified Bessel functions $\Re_1$ and $\Re_2$ do not contribute significantly. Thus, in an attempt to bring out the unsteady terms, an example was undertaken using an extremely large value of reduced frequency, $k_r=8.7554$.§ At this frequency unsteady effects are expressed by the slight dipping of the curve below the abscissa. A second interesting feature of these comparisons is that the calculated results using the Doublet-Lattice Method do not show these slight dips in the curves. The reason for this is that the approximating functions used for the kernel in the *DLM* do not have the exact limiting behavior, for small values of $\bar{z}$ as do the Bessel functions. The approximating function is made up of a series of exponential terms. This function fits the Bessel function well but ultimately has an exponential character for small $\bar{z}$. This peculiarity does not present a practical difficulty. For example at the reasonable value of reduced frequency of $\pi/2$, the maximum error is approximately 0.045 percent of the planar contribution (see Fig. 5a).

A further application of the refined algorithm is to the T-tail oscillating in yaw tested at low-speed by Clevenson and Leadbetter.[11] The magnitude $|C'_{l,\psi}|$ and phase angle $\phi'_{l,\psi}$ of the rolling moment of the horizontal stabilizer was presented in Ref. 1 using the original algorithm. The calculations took the ground effect of the wind-tunnel floor into account simply by doubling the height of the fin. Forty boxes were placed on the fin and its reflection (5 chordwise on 8 spanwise strips) and 40 boxes were placed on the horizontal stabilizer semispan (also 5 chordwise on 8 spanwise strips). The experimental data and the calculations for $M=0$ of Ref. 1 are reproduced in Fig. 6. A later study, using the original algorithm,[8] investigated the convergence by using 50 boxes on the fin (5 chordwise on 10 spanwise strips) and 50 boxes on the stabilizer (also 5 chordwise on 10 strips) as shown in Fig. 6. Also, the ground effect was accounted for by reflecting the complete configuration. The effect of Mach number (up to $M=0.50$) was included in the calculations. The results of Ref. 8 showed the solution of Ref. 1 to have converged, and that the ground effect of the horizontal

§ This value of k_r results in the downwash being 90° out-of-phase with the bound vortex, i.e., $\exp(-i\omega x_0/U)=i$.

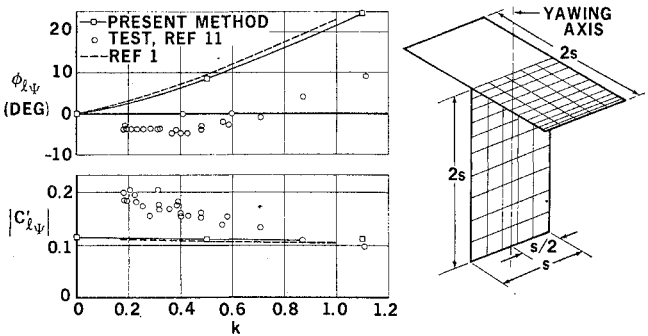

Fig. 6 Rolling moment coefficient of horizontal stabilizer for simplified T-tail oscillating in yaw about fin mid-chord.

stabilizer and Mach number effect are negligible at the reduced frequencies ($0.09 \leqslant k_r \leqslant 0.56$) tested. It was not anticipated that the refined algorithm would result in any substantial change since the effect of the refinement should be limited to the region of the fin-stabilizer intersection. The new results for 100 boxes are also shown in Fig. 6 for a complete reflection and an average Mach number of the wind-tunnel test of $M = 0.3$. The new results show no significant change other than an improved convergence.

References

[1] Albano, E. and Rodden, W. P., "A Doublet-Lattice Method for Calculating Lift Distributions on Oscillating Surfaces in Subsonic Flows," *AIAA Journal*, Vol. 7, No. 2, Feb. 1969, pp. 279–285; also Errata *AIAA Journal*, Vol. 7, No. 11, Nov. 1969, p. 2192.

[2] Vivian, H. T. and Andrew, L. V., "Unsteady Aerodynamics For Advanced Configurations; Part I—Application of the Subsonic Kernel Function to Nonplanar Lifting Surfaces," FDL-TDR-64-152, May 1965, Air Force Flight Dynamics Lab., Wright-Patterson Air Force Base, Ohio.

[3] Landahl, M. T., "Kernel Function for Nonplanar Oscillating Surfaces in a Subsonic Flow," *AIAA Journal*, Vol. 5, No. 5, May 1967, pp. 1045–1046.

[4] Kalman, T. P., Rodden, W. P., and Giesing, J. P., "Application of the Doublet-Lattice Method of Nonplanar Configurations in Subsonic Flow," *Journal of Aircraft*, Vol. 8, No. 6, June 1971, pp. 406–413.

[5] Balcerak, J., "Flutter Tests of Variable Sweep Configurations," AFFDL-TR-101, Sept. 1968, Air Force Flight Dynamics Lab., Wright-Patterson Air Force Base, Ohio.

[6] Albano, E., Perkinson, F., and Rodden, W. P., "Subsonic Lifting-Surface Theory Aerodynamics and Flutter Analysis of Interfering Wing/Horizontal-Tail Configurations," AFFDL-TR-70-59, May 1970, Air Force Flight Dynamics Lab., Wright-Patterson Air Force Base, Ohio.

[7] Giesing, J. P., Kalman, T. P., and Rodden, W. P., "Subsonic Unsteady Aerodynamics for General Configurations; Part I, Direct Application of the Nonplanar Doublet-Lattice Method," AFFDL-TR-71-5, Feb. 1971, Air Force Flight Dynamics Lab., Wright-Patterson Air Force Base, Ohio.

[8] Kalman, T. P., Rodden, W. P., and Giesing, J. P., "Aerodynamic Influence Coefficients by the Doublet-Lattice Method for Interfering Nonplanar Lifting Surfaces Oscillating in a Subsonic Flow," DAC-67977, Nov. 1969, Douglas Aircraft Co., Long Beach, Calif.

[9] Hedman, S. G., "Vortex Lattice Method for Calculation of Quasi Steady State Loadings on Thin Elastic Wings," Rept. 105, Oct. 1965, Aeronautical Research Inst. of Sweden, Stockholm.

[10] Mangler, K. W., "Improper Integrals in Theoretical Aerodynamics," Rept. Aero 2424, C. P. No. 94, June 1951, Royal Aircraft Establishment, Farnborough, Hants, England.

[11] Clevenson, S. A. and Leadbetter, S. A., "Measurements of Aerodynamic Forces and Moments at Subsonic Speeds on a Simplified T-tail Oscillating in Yaw About the Fin Mid-Chord," TN 4402, 1958, NACA.

[12] Rodden, W. P., Giesing, J. P., and Kalman, T. P., "New Developments and Applications of the Subsonic Doublet-Lattice Method for Nonplanar Configurations," AGARD-CP-80-71, Paper No. 4, *AGARD Symposium on Unsteady Aerodynamics for Aeroelastic Analyses of Interfering Surfaces*, Tønsberg, Oslofjorden, Norway, Nov. 3–4, 1970.